Petroleum Science 21 (2024) 2370–2382

Contents lists available at ScienceDirect

Petroleum Science

journal homepage: www.keaipublishing.com/en/journals/petroleum-science

Original Paper

Rock physical characteristics of deep dolomite under complex geological conditions: A case study of 4th Member of Sinian Dengying Formation in the Sichuan Basin, China

Chuang Li [a, *], Shu-Xin Pan [a], Hong-Bin Wang [a], Ji-Xin Deng [c], Jian-Guo Zhao [b], Zhi Li [b], Yu Zhang [b]

[a] Northwest Branch of Research Institute of Petroleum Exploration & Development, Lanzhou, 730020, Gansu, China
[b] State Key Laboratory of Petroleum Resources and Engineering, China University of Petroleum (Beijing), Beijing, 102249, China
[c] Department of Geophysics and Exploration, College of Geophysics, Chengdu University of Technology, Chengdu, 610059, Sichuan, China

ARTICLE INFO

Article history:
Received 22 March 2023
Received in revised form
19 December 2023
Accepted 20 March 2024
Available online 7 April 2024

Edited by Jie Hao and Meng-Jiao Zhou

Keywords:
Deep-ultra deep carbonate reservoirs
Rock physics properties
Dolomite
Seismic elastic properties
Micro-crack
Pore structure types

ABSTRACT

The deep-ultra deep carbonate reservoir in China, commonly subjected to modification of multi-stage diagenesis, has extremely high heterogeneity. Conventional rock physics analysis cannot accurately identify the elastic responses of reservoir. Here, the rock physics properties of the dolomite from the 4th Member of the Sinian Dengying Formation are experimentally measured, and the change law of rock physics characteristics is investigated within the framework of the diagenetic processes by the analysis of the elastic and petrologic characteristics, pore structure, and sedimentary environments. The results show that the differentiated diagenesis results in different pore structure characteristics and micro-texture characteristics of the rock. The microbial dolomite of the algal mound-grain beach facies is subjected to the contemporaneous microbial dolomitization and seepage-reflux dolomitization, pene-contemporaneous selective dissolution, burial dolomitization, and hydrothermal dolomitization. The resultant crystalline dolomite is found with one main type of the dolomite crystal contact boundaries, and the dissolution pore is extensive development. The siliceous, muddy, and limy dolomite of the inter-beach sea environment mainly experiences the weak capillary concentration dolomitization, intensive mechanical compaction-induced densification, and burial dolomitization. Such crystalline dolomite is observed with four types of contact boundaries, namely the dolomite contact, clay contact, quartz contact, and calcite contact boundaries, and porosity mostly attributed to residual primary inter-granular or crystalline pores. The samples with the same crystal boundary condition have consistent correlations between the compressional- and shear-wave velocities, and between the compressional-wave velocity and the velocity ratio. Additionally, the variation of the acoustic velocity with effective pressure and the intensity of pore-scale fluid-related dispersion are controlled by the differentiation of pore structure types of the samples. The varied effects of soft pores like micro-cracks on the compressional- and shear-wave velocity causes considerable changes in the relationships between the compressional- and shear-wave velocities, compressional-wave velocity and velocity ratio, and porosity and acoustic velocity. This research is an attempt to demonstrate a novel method for investigating the rock physics variation of rock during the geological process, and the obtained findings can provide the rock physics basis for seismic prediction of the characteristics of deep carbonate reservoirs.

1. Introduction

Great oil and gas exploration potential was found in the deep (with burial depth >4000 m) and marine carbonate reservoirs of China (Zhao et al., 2012; Ma et al., 2020). Over recent years, numerous deep carbonate oil and gas fields, such as Anyue,

* Corresponding author.
E-mail address: lichuang@petrochina.com.cn (C. Li).

https://doi.org/10.1016/j.petsci.2024.03.015

Tazhong, Longgang, and Shunbei, had been discovered and developed successively (Jin and Cai, 2006; Ma et al., 2019a, 2019b). The marine deep carbonate reservoir had become the most advantageous strata for hydrocarbon exploration and exploitation in China and also a practical supporter of China's energy relay.

Determining reservoir characteristic parameters, such as lithology, physical properties, and gas-bearing properties, via a seismic prediction approach were always an important content and basis for exploration target evaluation of deep carbonate reservoirs. However, with the increase of depth, the rock was becoming increasingly tight and the reservoir characteristics changes. The resultant reduced differentiation of seismic responses, together with the degraded quality of seismic data of deep formations, greatly challenges the seismic prediction of deep-ultra-deep carbonate reservoirs (Ma et al., 2020; He et al., 2021). Given this, scholars had carried out targeted studies, which result in much important progress. Research shows that rock physical properties of carbonate rocks were affected by multiple factors such as the rock texture, pore structure, porosity and pore fluids. Ultrasonic measurement of carbonate rocks and observation of their microscopic structures have demonstrated the difference in pore types was the main contributor to obvious disparity of acoustic velocities between carbonate rock samples with similar porosity (Anselmetti and Eberli, 1999; Weger et al., 2009; Wang et al., 2015b; Xie et al., 2022). With the help of the theoretical model of the cracked porous media and the multi-frequency rock physics tests of carbonate rock samples, the influences of the pore structure and pore fluid on the elastic wave velocity, elastic modulus, anisotropy, frequency dispersion, and attenuation characteristics were analyzed, and a reservoir seismic prediction method based on elastic parameters and frequency-dependent attenuation attributes was developed (Yin et al., 2015; Deng et al., 2015a, 2015b; Wang et al., 2015a, 2015b; Li et al., 2019; Wang et al., 2021; Guo et al., 2022; Liao et al., 2023). Through the seismic forward numerical simulation of the cracked porous rock media, the seismic response patterns of the rock characteristics, such as carbonate rock framework, pore structure and pore fluids were investigated (Ba et al., 2011; Zhao et al., 2013; Kong et al., 2013; Hu et al., 2016; Li et al., 2023), and the relationship between the wave field information and reservoir parameters was identified, which laid down a basis on the seismic wave field response mechanism for seismic prediction of the lithology, pore structure, and pore fluid of carbonate reservoirs.

The high cost of deep carbonate exploration and development raised the requirement on the accuracy of seismic prediction of reservoir characteristics, and the seismic rock physical properties of the reservoir rock were the key bridge connecting reservoir parameters with seismic response features. Therefore, the key to predicting reservoir parameters by artificial seismic was to accurately understand the seismic rock physical characteristics of deep marine carbonate reservoirs, and to establish the quantitative relationship between reservoir parameters and seismic elastic and inelastic parameters by means of correlation analysis. Deep marine carbonate reservoirs in China present various sedimentary types and were typically subjected to the modification of multi-stage diagenesis, so they were found with high complexity in pore structures and strong heterogeneity (Ma et al., 2020; He et al., 2021), which made it difficult to accurately capture the overall rock physical variation pattern of reservoir rock and clarify the geological implication of the change of rock physical characteristics via a rock physics analysis failing to sufficiently incorporate the geological setting. Therefore, for deep marine carbonate reservoirs, it was necessary to not only analyze and summarize the seismic rock physical regularity, based on high-temperature high-pressure tests but also study the geological factors controlling the changes of the rock physical properties within the framework of the sedimentary environments-diagenetic processes-rock characteristics. By doing so, one was able to objectively and accurately identify the relationships between the seismic parameters and reservoir geological parameters (the sedimentary facies, lithology, pore structure, pore fluid, etc.) and assign the former with the deterministic geological implications. Given the aforementioned, the deep dolomite reservoir of the 4th Member of the Sinian Dengying Formation (Z_2dn_4) in the Hechuan-Tongnan area of the Sichuan Basin was taken as an example in this research, of which the rock physical variation patterns were identified and the effects of the diagenetic difference on the reservoir rock physical characteristics were investigated, by systematically measuring the petrologic and pore structure features, and physical and seismic elastic properties of the reservoir, determining the sedimentary environment and clarifying the rock characteristic variation during diagenesis. This research, taking a specific deep carbonate reservoir as an example, is an attempt to develop and demonstrate a novel seismic rock physical research method for chemical sedimentary rock and provide a scientific basis for effective seismic evaluation of deep marine carbonate reservoirs.

2. Geological background

The Hechuan-Tongnan area was located in the Gaoshiti-Moxi block adjacent to Anyue gas field in the central-western Sichuan Basin, and the transition zone of the gentle structural area of the Chuanzhong (Central Sichuan) paleo-uplift and Chuandongnan (Southeast Sichuan) highly-steep structural area (Wang et al., 2016; Chen et al., 2017), as depicted in Fig. 1. The Sinian Dengying Formation is widely distributed across the study area, which is found with conformity with the underlying Sinian Doushantuo Formation and yet unconformity with the overlying mudstone and shale of the Cambrian Qiongzhusi Formation. According to the lithologic groups and electrical characteristics, the Dengying Formation can be divided into four lithologic members from bottom to top, namely the 1st (Z_2dn_1), 2nd (Z_2dn_2), 3rd (Z_2dn_3) and 4th (Z_2dn_4) Members (Fig. 1). The Z_2dn_1 Member is mainly light gray-dark gray blocky dolomicrite under the sedimentary environment of the intra-platform beach and the inter-beach sea, with the thickness of 20–150 m, and the bacteria and algae fossils rich microbial dolomite is scarce. The Z_2dn_2 Member is dominated by light gray-gray block microbial dolomite with enrichment of algae fossils and with grape texture developmented, deposited in the lagoon and tidal flat environments with a thickness of 350–530 m. The Z_2dn_3 Member is gray-black shale interbedded by silty sandstone, formed in the shelf sedimentary environment, with a thickness of less than 60 m. The Z_2dn_4 Member consists of the block microbial dolomite, dolomicrite and siliceous rock, developing in the sedimentary environments of the intra-platform beach, lagoon, or inter-beach sea, with a thickness of 90–350 m. A set of high-gamma-ray siliceous-banded dolomite with high shale content or siliceous rock occurs in the middle of the Z_2dn_4 Member. By this siliceous bed, the Z_2dn_4 Member can be subdivided into the upper and lower sub-members, and the upper sub-member of Z_2dn_4 is the main gas pay zone of the Dengying Formation in the study area.

At the end of the Dengying period, the differential uplifting of the Tongwan Movement EpisodeIlleads to the considerable uplifting of the study area (Yang et al., 2020; Jiang et al., 2023). Due to the large-scale penecontemporaneous karstification, the Z_2dn_4 Member commonly suffers from leaching and dissolution by meteoric freshwater, which results in selective development of dissolution pores and significant improvement of the reservoir petrophysical properties. Afterward, the study area successively experiences the Caledonian, Hercynian, Indosinian, Yanshanian, and Himalayan tectonic movements, which leads to the uneven development of

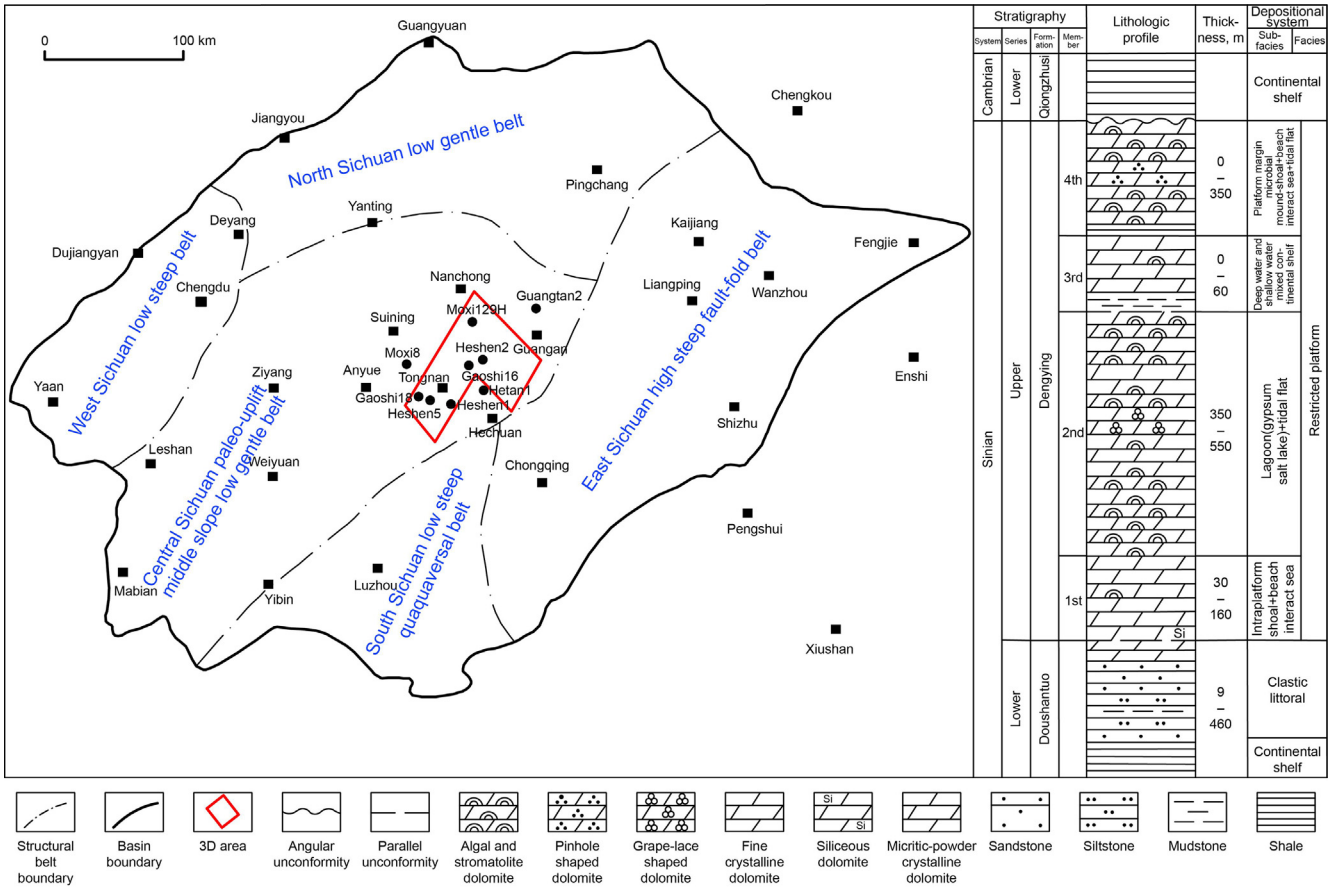

Fig. 1. Location of the study area and stratigraphic histogram of Dengying Formation.

multi-stage fractures in the dolomite reservoirs, connecting the earlier dissolution pores, further improving reservoir petrophysical properties, and also providing flow channels for later hydrothermal activities.

3. Sample preparation and experimental methodology

A total of 200 core plus were taken from cores in wells HS 2, HS 5, GS 16, GS 18 and GS 21. The cored rock samples all had a diameter of 25.4 mm and height surpassing 60 mm, which were then cut and prepared into core cylinders with height of 35–55 mm and inclination below 0.05 mm for testing petrophysical and seismic elastic properties. The leftover sample from cutting was used for the X-ray diffraction whole-rock mineral analysis (PANalytical (Empyrean) X-ray diffractometer), optical thin-section analysis and scanning electron imaging (Quanta250 FEG). Some thin sections were stained with Alizarin Red S to distinguish dolomite from calcite. A total of 50 representative samples were powder for stable C and O isotopes measurement by using a Mess und Analysen-Technik (MAT) 252 mass spectrometer, and the standardized data were converted to Vienna Peedee belemnite (VPDB). Porosity and permeability of the core samples was tested using the pulse decay gas-based method (CMS-300 Automated Permeameter). The pore structure characteristics of the rocks were analyzed by an industrial CT scanning imaging system, which adopted the German Phoenix micro-focus X-ray industrial CT with a detail resolution of up to 1 μm.

The ultrasonic transmission technique was employed to measure velocity (Deng et al., 2015a, 2015b). A time gap of 15 min was set between measurements at each pressure point so as to ensure the equilibrium of the pore pressure of the sample with the confining pressure. The sample was first being dried in a drying oven for 48 h at 70 °C, to make the sample reach a "relatively" dry condition (in which the sample only contains crystal water and clay-bound water). Then the dried sample was placed in humid open air for more than 24 h, so that the sample contained about 2%–3% of water to compensate the damage to the rock framework induced by clay mineral dehydration. Water saturated samples were achieved by imbibition method under confining pressure of 5 MPa. The experiment pressure increased from 2 to 60 MPa, during which measurement was carried out at the interval of 5 MPa. The pressure deviation was less than 0.3%. The central frequency of the P-wave transducer for the apparatus was 800 kHz, while that of the S-wave transducer was 350 kHz. The time measurement error of the oscilloscope was less than 0.01 μs, and in other words, the relative errors of velocity measurement of the test apparatus were about 1% for P-wave and 2% for S-wave.

4. Results and analysis

4.1. Petrological characteristics

The core and thin section observation shows that the lithology of the reservoir mainly includes stromatolite algal/laminar algal/bonded algae/thrombolite dolomite of the intraplatform mound subface, and dolarenite/coarse-crystal dolomite of intraplatform beach subface, and micritic/clay-bearing/gypsum-bearing/siliceous/calcareous dolomite of inter-beach sea subface. The mineral composition of reservoir rocks is mainly composed of dolomite, followed by quartz, clay minerals, calcite, and a small amount of pyrite. The laminar algal dolomite is gray and stratified, and

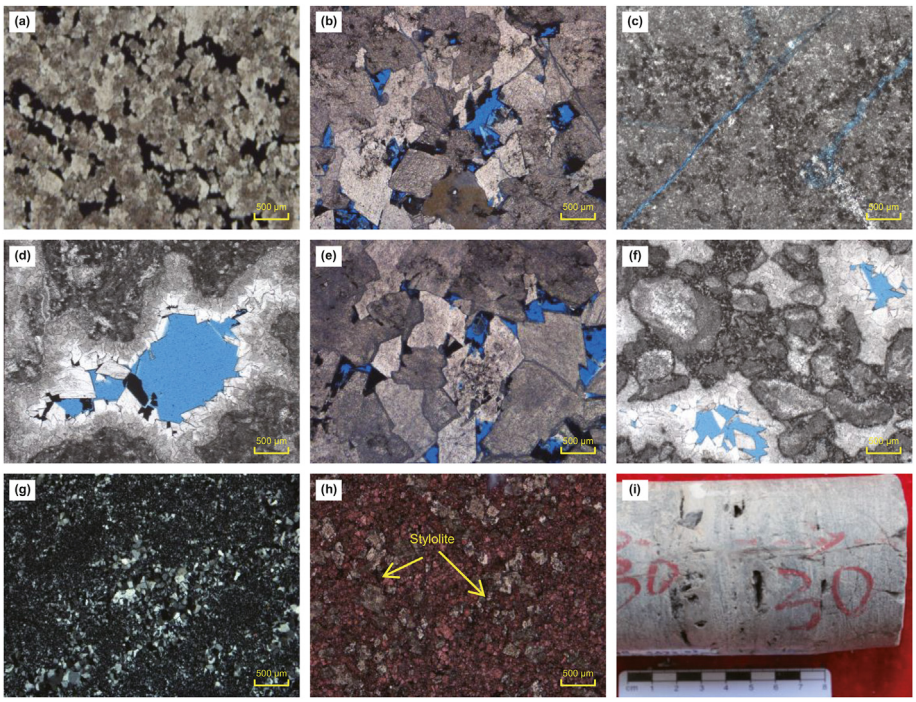

Fig. 2. Lithology and reservoir space characteristics of dolomites in the Z_2dn_4 in Sichuan Basin. **(a)** Well HS 2 (5493.1 m), silty-to fine crystalline dolomite, residual algae-framework pores; **(b)** well GS 16 (5453.6 m), stromatolite dolomite, dissolution pores and micro-crack development; **(c)** well HS 5 (5348.1 m), algae-bonded dolomite, micro-crack development; **(d)** well HS 5 (5341.1 m), algae-bonded dolomite, dissolution pores development; **(e)** well HS 5 (5414.2 m), thrombolite dolomite, dissolution pores development; **(f)** well HS 5 (5342.3 m), algae dolarenite dolomite , inter-crystalline pores development; **(g)** well GS 16 (5478 m), siliceous dolomite; **(h)** well GS 16 (5449.7 m), calcareous dolomite (Alizarin red staining, calcite is red in color); **(i)** well HS 2 (5509.4 m), dissolution pores developed along the beddings of stromatolite dolomite.

relatively flattened, with inferior lateral continuity and a thin layer of silty dolomite between laminar, formed by benthic microflora (mainly the Cyanobacteria) capturing and bonding clastic sediments; under the microscope, the dolomite shows the crystal grain texture or residual granular texture, with the grains mainly composed of subhedral-euhedral silt-size-to fine (some medium) crystalline dolomite showing the granular mosaic texture, dirty crystal surface, representing a low-energy tidal flat environment (Fig. 2(a)). Stromatolite algal dolomite is gray and medium thickness with continuous algae-rich dark laminations and algae-lean bright laminations that are arranged in an interlaminated manner with consistent fluctuation; in the thin section images, it is shown that the dolomite crystal mainly present the granular texture, with the residual and unidentifiable laminae both observed in the samples; the grains are mainly composed of euhedral-subhedral-anhedral fine-to medium crystalline dolomite with the granular mosaic texture, interpreted as a medium-low energy depositional environment from the lower intertidal zone to the upper subtidal zone (Fig. 2(b)). The algae-bonded dolomite is light gray-gray in color and occurs mainly as massive dolomite, and the remains of algae can be seen in both core specimens and thin section images. The thrombos formed by algae-bonded clastic particles are extremely irregular in distribution. The microscopic observation shows that the algae-bonded dolomite is characterized by the micritic texture; algae-rich micrite deforms under compression and penetrates clastic particles to form clots Fig. 2(c)–(d). The thrombolite dolomite and algae dolarenite dolomite both belong to granular rock, which, by definition, are composed of dolomicritic detritus with a grains size larger than 2 mm and ranging between 0.125 and 2 mm, respectively. They, subjected to intensive recrystallization, are found under the thin section images as mainly composed of subhedral-euhedral medium-to coarse crystalline dolomite with dirty crystal surfaces, showing the granular mosaic texture, and unidentifiable algae morphology Fig. 2(e)–(f). The light gray massive micritic dolomite shows the anhedral mosaic texture. It may contain clay minerals and quartz of the sedimentary origin Fig. 2(g)–(h), and can also develop into the siliceous-layer dolomite (Fig. 2(g)). It represents an area within the restricted platform with relatively deep water depths, which is thus rarely affected by tides or waves. At last, the dark gray massive calcareous dolomite is seen with the distribution of the dark, spotted dolomite along the stylolite seams Fig. 2(h), and the subhedral-anhedral silty-to fine dolomite grains coexists and is intergrown with the surrounding light-colored limestone. In the calcareous dolomite, it is generally separated from the matrix limestones by stylolite seams, and dolomite grains with cloudy centers and clear rims occur locally in the matrix limestone.

According to the core observation and well-logging characteristics, the Z_2dn_4 in the study area consists of two short-period mound-shoal composite complex, and each short-period cycle is similar in the lithologic association. The lithology of a complete sedimentary cycle from bottom to top is as follows: tight micritic/clay-bearing/gypsum-bearing/siliceous/calcareous dolomite of inter beach sea depositional environment, stromatolite algal/laminar algal/bonded algae/thrombolite dolomite of the intraplatform mound depositional environment, and dolarenite/coarse-crystal dolomite of intraplatform beach depositional environment. Due to the differentiated seal level variation, not all sedimentary cycles present the complete development of the above three lithologic associations, and meanwhile, the characteristic of “large beaches and small mounds” is observed.

4.2. Pore structure characteristics

The pore types of the Z_2dn_4 reservoir can be divided into fabric-selective pores formed during depositional and non-fabric-

selective pores formed during diagenesis stage (Choquette and Pray, 1970). Fabric-selective pores are mainly primary pores occurring during depositional stage, such as algae-framework pores and biological skeleton/shell cavity (body cavity) pores in algae-rich sediments Fig. 2(a), and inter-granular pores in granular sediments, which are prone to cementation by early cement. Yet, the residues of such pores provide the basis for penecontemporaneous dissolution. The pores formed during diagenesis include the inter-crystalline pores formed by Mg^{2+} with a smaller ion radius replacing the larger Ca^{2+} during dolomitization Fig. 2(b)–(f), and inter- and intra-granular dissolution pores formed by penecontemporaneous, supergenic, and burial dissolution Fig. 2(b)–(d). The penecontemporaneous dissolution include the sediment of low-temperature dolomite with low degrees of order, aragonite, or calcite matter by meteoric or mixed water, which results in the enlargement of primary matrix pores to form the dissolved pores and vugs by further dissolution, especially the fabric-selective dissolution Fig. 2(i). The penecontemporaneous dissolution is controlled by frequent eustacy. This explains the phenomena observed on cores that dissolved pores and vugs with size of 1–10 mm closely distribute along layers at the upper part of the upward shallowing cycle related to the depositional exposure surface, and the gypsum moldic pores related to the exposure evaporation are also observed, which both indicate that penecontemporaneous dissolution is the most important instructive pore-forming process of the dolomite reservoir in the study area. Supergenic karstification refers to the dissolution of dolomite in the reservoir by meteoric water, after the reservoir is uplifted to the surface. During this process, the dolomite minerals have all been highly stabilized and the formation exposure time is short, so the contribution of dissolution to porosity is lower than that of the penecontemporaneous dissolution. The burial environment could generate a small amount of dissolved pores through the dissolution of organic acids and TSR (sulfate reduction reaction) (Zhang et al., 2011). As a typical evidence of hydrothermal dissolution, quartz cement can be dissolved to bay-like pore. However, pores are more often filled with hydrothermal minerals such as quartz, saddle dolomite, fluorite, and pyrite Fig. 2(d)–(f). This implies that the burial-hydrothermal activity has both contributions to reservoir porosity by dissolution and negative influences by plugging early pores due to hydrothermal precipitation, especially the pore filling and metasomatism of a large number of hydrothermal anhedral quartz crystals that are greatly harmful to the reservoir pore space. Because of the dependence of dissolution on primary pores, the dissolution pores are more developed in the dolomite reservoir of the algae-rich mound-shoal burial environment. While the micrite dolomite of the inter beach sea depositional environment lacks primary pores, resulting the weak development of dissolution pore, and the rock is very tight. The pores in micrite dolomite are mainly the residual inter-crystalline pores and inter-granular pores. Multi scale fractures, mainly micro-cracks Fig. 2(b)–(c) are extensively developed in the Z_2dn_4 reservoir of the study area, but the distribution of cracks is extremely uneven in the vertical and horizontal directions.

According to the differences of the reservoir pore space characteristics of reservoir rock in the Z_2dn_4, four main reservoir pore types are identified, namely the crack-dissolution vugs, dissolution vugs, crack-pore, and pore-dominated types. The reservoirs of the crack-dissolution vug and dissolution vug types mainly occur in the algal dolomite and granular dolomite of the mound-shoal facies, which is found (in CT imaging slices) primarily with medium and large dissolution vugs with diameters above 2 mm and micro pores less than 1 mm and straight or curved micro cracks at difference scales connecting such dissolution vugs Fig. 3. Moreover, the flower-like pore throat combination is staggered and stacked over each other and extends towards the surrounding, which is also beneficial to the connection of dissolution pores at different scales Fig. 3(d). The reservoirs of the crack-pore and pore-dominated types typically develop in the dolomite of the inter beach sea depositional environment. The corresponding CT imaging slice shows suppressed development of dissolution pores and the reservoir space mainly composed of micro pores between 0.01 and 1 mm. Furthermore, it is observed that the crack development scale is small and discontinuous Fig. 4(c); the relatively isolated pore throat is seen with localized overlap and short extension, which is thus associated with poor communication among pores Fig. 4(d).

4.3. Petrophysical properties

Porosity of the Z_2dn_4 dolomite samples of the study area mainly

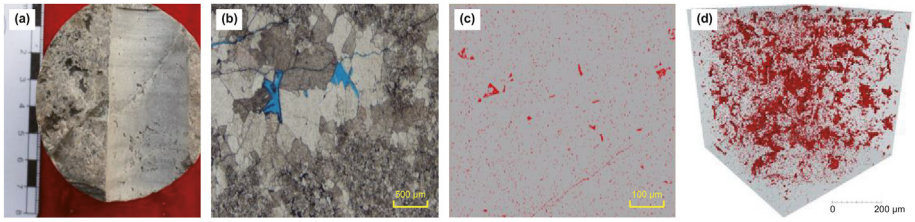

Fig. 3. Multi-scale pore structure characteristics of dolomite samples with crack-dissolution vug type in Z_2dn_4. **(a)** Well HS 2 (5489.2 m), core; **(b)** the development of dissolution pores and micro-crack in the cast thin section; **(c)** micron CT section, micro-cracks communicate with dissolution pores; **(d)** 3D CT display of pore-throat.

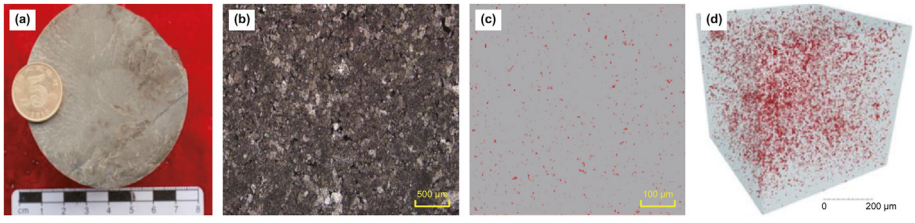

Fig. 4. Multi-scale pore structure characteristics of dolomite samples with dissolution vug in Z_2dn_4. **(a)** Well HS 2 (5587 m), core; **(b)** residual inter-crystalline pores were observed in the cast thin section; **(c)** micron CT section, inter-crystalline pores; **(d)** 3D CT display of pore-throat.

ranges from 0.1% to 8%, with an average of 2.6%, and the samples with porosity greater than 4% account for 20% of the total samples. The corresponding permeability is 0.016–14.5 mD, averaging 3.96 mD. Furthermore, the average permeability of the samples with porosity above 4% is 6 mD, and the permeability can change by 2–6 orders of magnitude at the same porosity. The porosity versus permeability shows that the porosity and permeability are poorly correlated, with only a weak overall positive correlation Fig. 5(a). As stated above, the pores of the deep dolomite in the Z_2dn_4 are mainly derived from the inheritance of primary pores and penecontemporaneous dissolution, which cause the porosity of the algal dolomite and granular dolomite of the mound-shoal environment greatly higher than that of the argillaceous dolomite, siliceous dolomite, and calcareous dolomite of the inter-beach sea environment, but corresponding permeability shows apparent overlap. The porosity and permeability of crack-dissolution vugs and dissolution vug samples vary from 3.5% to 7.2% and 0.016 to 191.2 mD, respectively. The positive correlation between porosity and permeability of the crack-dissolution vugs samples is considerably higher than that of the dissolution vug samples, and the permeability of the two type samples can vary by 2–3 orders of magnitude with the same porosity. The porosity of the crack-pore and pore-dominated type samples lies between 0.1% and 3.5%, and correspondingly, the permeability varies from 0.0003 mD to 95.2 mD. The positive correlations between porosity and permeability of the two type samples are consistent, and the permeability shows a larger variation by 3–6 orders of magnitude at same porosity. Due to the well development and extension of pore-throats and the predominance of larger throats of 0.5–3 μm in the dissolution vug and crack-dissolution vug Fig. 3(d), the connection with the dissolution pore is improved by the good pore-throat coordination. This is embodied as that the crack and pore-throat both serve as fluid flow channels; the development of micro cracks can effectively improve permeability, and yet is not the only contributor to permeability enhancement. The pore-throat development and extension are inferior in the pore-dominated and crack-pore samples, dominated by small throats of 0–0.06 μm Fig. 4(d); the pore-throat coordination is low, and the pore-throat connection is insufficient. For those samples, only cracks serve as the main fluid flow channels, associated with the crack-dependent linear porosity-permeability correlation, and the apparent permeability difference between samples with and without micro fractures.

4.4. Seismic rock physical properties

The relationships between the acoustic velocity and pressure for the dried and saturated samples with the four typical pore-structure combinations are illustrated in Fig. 6. The P- and S-wave velocities of samples present two increasing trends with the increase of effective pressure. Specifically, the pore-dominated dolomite, on the one hand, is seen with the near-linear slow acoustic velocity increase along the whole pressure range. Such samples feature the simple pore types, mainly of residual intercrystalline and granular pores with uniform mechanical properties, which gradually deforms to the pore shapes with higher stiffness under pressure to generate nearly identical growth of the equivalent elastic modulus of the rock medium. On the other hand, for the crack-dissolution vug, dissolution vug, and crack-pore dolomite samples, two features are observed, namely the nonlinear rapid increase under low pressure and linear slow increase under high pressure. The above three types of samples are found endowed with the "dual-porosity" texture, composed of less-rigid micro cracks and more-rigid dissolution pores. With the increase of effective pressure, crack in the rock samples gradually close, from less rigid ones to rigid ones successively.

The effective modulus growth of the rock medium induced by the closure of micro cracks with smaller rigidity is greater than that of pores and vug with larger rigidity, and hence nonlinear rapid rising of the acoustic velocity is observed under low pressure. As the pressure grows to a certain value, the cracks are completely closed, and the rock medium can be regarded as being composed of dissolution pores or pores with higher rigidity (compared with cracks). The further increase of pressure mainly leads to the gradual uniform deformation of stiff pores, which results in the linear acoustic velocity variation trend with pressure. For samples with dissolution vug, the nonlinear acoustic velocity increase under low pressure is related to the existence of pore throats or compliant grain contact boundary with relatively low rigidity. However, because of the low content of such compliant pore, the corresponding acoustic velocity variation magnitude of dissolution vug samples with pressure is smaller, compared with the other two typical "double-porosity" dolomite. So, dissolution vug can be regarded as a transitional type between the crack-dissolution vug and crack-pore dolomite, and pore-dominated dolomite, in terms of the acoustic velocity-pressure relationship. The influence of the pore type differences on the acoustic velocity is also reflected in the velocity change after the fluid saturation. The P-wave velocities of all samples increase by different degrees after water saturation, compared with those of the dry condition. Nonetheless, the velocity increase of the crack-dissolution vug and crack-pore samples with "dual-porosity" is higher, and meanwhile, the measured velocity values of these two types under low effective pressure are considerably higher than the Gassmann equation's predicted results (Mavko et al., 2023). These indicate that the influence of pore-

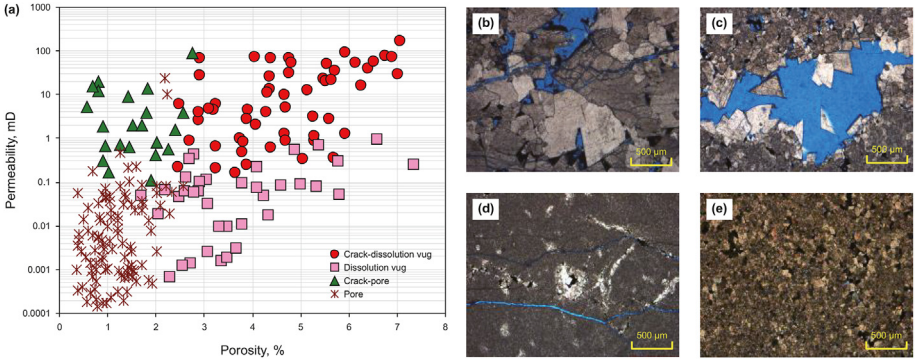

Fig. 5. Crossplot of total porosity versus permeability and micrographs of pore types of dolomite samples in Z_2dn_4. **(a)** Projection diagram of porosity-permeability; **(b)** crack-dissolution vug dolomite; **(c)** dissolution vug dolomite; **(d)** crack-pore dolomite; **(e)** pore-dominated dolomite.

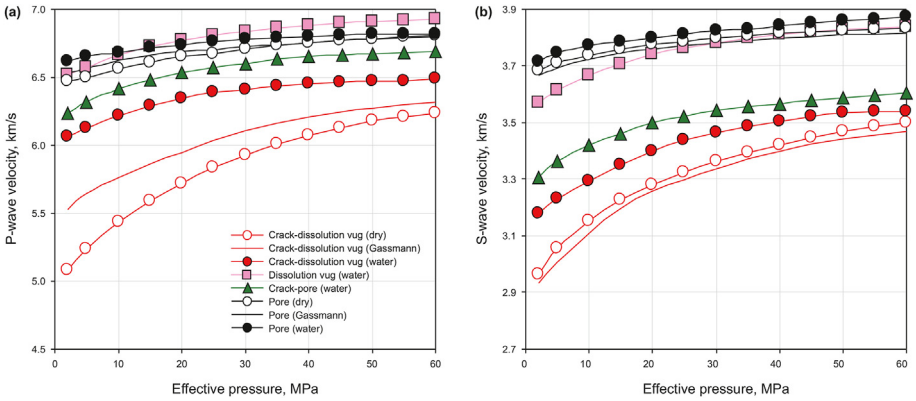

Fig. 6. V_p versus effective pressure **(a)** and V_s versus effective pressure **(b)** of dolomite samples with different pore types in Z_2dn_4.

scale fluid-related dispersion on the velocity at the ultrasonic frequency, and the magnitude of such dispersion effects is dependent on the pore stiffness differentiation in the rock media. For the pore-dominated samples with a simple combination of pore types, the pore-scale fluid-related dispersion is reduced by the homogeneous porous elastic properties, the measured velocities are close to the calculated ones based on the Gassmann equation, and the S-wave velocity of the dry samples is slightly higher than that of the water-saturated sample. Due to the presence of pore throats with small rigidity, which can also lead to the porous elastic property differentiation under low effective pressure, the experimental results of the dissolution vug samples are to some extent different from the calculated velocities based on the Gassmann equation. With the increase of confining pressure, the pore stiffness tends to be uniform with the gradual closure of micro fractures. Under such circumstances, the pore-scale fluid flow induced by elastic waves lacks the pore structure basis for occurring, and accordingly the gap between the measured P-wave velocity of these “dual-porosity” samples and the Gassmann equation's predicted results is gradually narrowed.

The variation of the P- and S-wave velocities with porosity of the dolomite samples of the Z_2dn_4 under the reservoir conditions is illustrated in Fig. 7. In order to compare the influences of pore structures on the acoustic velocity, the differential equivalent modulus model is used to compute the relationship between the acoustic velocity and porosity in cases of varied pore aspect ratios, which is also plotted in Fig. 8. It is shown that the acoustic velocity of dolomite samples is generally negatively correlated with the porosity, and yet the corresponding relationship cannot be quantitatively characterized using a single statistical model. Clearly, the acoustic velocity is affected by sample composition. The increasing content of quartz, calcite, and clay in the sample all leads to considerable declines of the P- and S-wave velocities. For the samples with relatively pure dolomite composition, with the same porosity, the maximum differences of the P- and S-wave velocities are 1000 and 500 m/s, respectively. These indicate that the pore structure, rather than porosity, is the primary factor controlling the acoustic velocity change of the Z_2dn_4 dolomite. We can also observe that P-wave velocities of dolomite samples are gradually close to the model line with the aspect ratio $\alpha = 0.01$. The aspect ratio of argillaceous dolomite and calcareous dolomite in the figure shows the characteristics of low aspect ratio, which is due to the mineral composition considered by the model line is the average value of dolomite samples, indicating that the elastic properties of rocks are the result of multiple factors. The effects of mineralogy and aspect ratio should be considered in the rock physics chart applied to seismic prediction.

5. Discussion

5.1. Diagenetic processes and rock textures

The paleoenvironment of Z_2dn_4 in the study area is generally located within a restricted platform (Du et al., 2015), and underwater uplifts of micro-geomorphology were only developed locally. Carbonate rock formation related to microbe is preferentially deposited in such higher parts during deposition. During transgression period, the rising of the sea level resulted in accelerated accretion and growth of the microbial mound in these higher parts. Consequently, the sedimentary body with the alternating uplift and low-lying land is formed, and fine-grained carbonate sediments containing argillaceous and terrestrial siliceous clasts were deposited in the low-lying land. The periodic eustacy leads to extensive development of microbial mound-shoal complex, with multi-stage vertical stacking.

The dolomite in the study area is of various geneses, and the superimposed modification of multi-stage dolomitization greatly increased the complexity of rock characteristics. The microbial dolomite is mainly considered to be the primary dolomite formed by precipitation of low-temperature dolomite related to microbial activities during (pene-)contemporaneous (Warthmann et al., 2005; Zhao et al., 2018). After the precipitation of primary dolomite, the algal dolomite including stromatolite algal, laminar algal and bonded algae, formed the rock frame with dolomicrite crystals, and such microbial dolomite is characterized by the well-preserved original rock structure and the development of T framework pore and intergranular pores Fig. 2(a). During the precipitation of low-temperature primary dolomite, foliaceous dolomite is the earliest generation of cement, which fills broadly in the framework pores as the results of seepage-reflux dolomitization Fig. 2(e)–(f). After the above-mentioned eogenesis, the rock framework of the microbial dolomite deposited in the intra-platform mound-shoal environment is almost completely consolidated. Assisted by the meteoric water, the penecontemporaneous dissolution further dissolves incompletely-consolidated and dolomitized sediments or dolomite with low degrees of order on the basis of the primary pore system. As a result, the primary pores are enlarged, and are also characterized by those apparent fabric-selective dissolution vugs along layers. In the subsequent burial process, due to the great increase of rock rigidity after eogenetic consolidation of dolomite, the effect of mechanical compaction is relatively reduced and compaction-related structures like stylolite are not developing. With the burial dolomitization, the recrystallization and overgrowth of dolomicrite crystals occur, which results in silty-to fine crystalline dolomite with partially preserved original rock textures such as

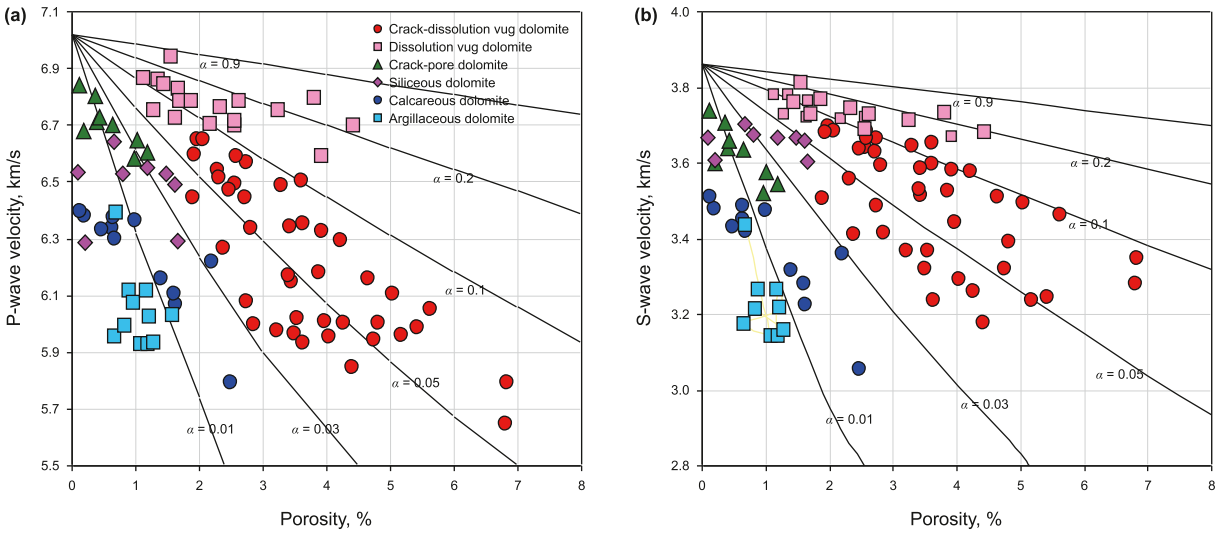

Fig. 7. P-wave velocity **(a)** and S-wave velocity **(b)** as function of porosity of samples in Z_2dn_4.

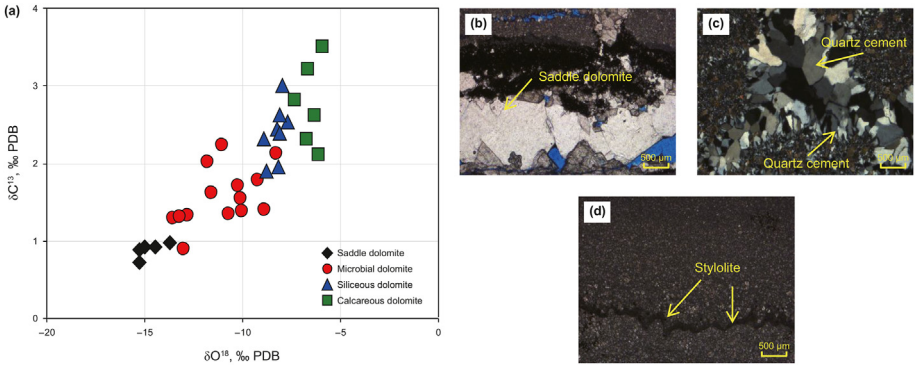

Fig. 8. Variation characteristics of δC^{13}–δO^{18} of dolomite samples in Z_2dn_4 **(a)**, saddle dolomite **(b)** and quartz **(c)** cementation due to hydrothermal dolomitization, and stylolite structure due to strong compaction of dolomite in inter-beach sea environment **(d)**.

residual algae laminae and algae particles. Also, it may produce fine-to crystalline dolomite and corresponding transition dolomite types that feature no residual original rock texture, due to the multi-stage replacement and recrystallization. As for thrombolite and dolarenite dolomite, they tend to form fine-medium granular dolomite without residual original rock textures. In the process of burial dolomitization, owing to the high porosity of the original rock, the crystal nucleus has sufficient space to grow freely during the recrystallization process. Thus, in the case of no hydrothermal dolomitization at higher temperatures, the euhedral-subhedral crystals are observed, with mosaic contact among crystallines. In addition to the early foliaceous dolomite cement, the pores are also found with cementation of hydrothermal minerals such as saddle dolomite, fluorite, pyrite, and quartz, which indicate the presence of hydrothermal dolomitization Fig. 2(b)–(c). Such hydrothermal dolomitization is mainly represented by associated saddle dolomite cement in pores and cracks, patchy anhedral dolomite cementation, and medium-coarse granular dolomite formed by burial dolomitization modification, or over-dolomitization, accompanied by the crystal shapes from subhedral-anhedral mosaic contact to anhedral mosaic contact Fig. 2(d)–(f). Due to the multi-stage dolomitization, the carbon stable isotope (δC^{13}) shows low positive value, and oxygen stable isotope (δO^{18}) exhibits high negative δO^{18} value Fig. 8(a), which reflects the influence of burial and hydrothermal dolomitization (Zhao et al., 2018). Also, both δC^{13} and δO^{18} value will shift to high negative values with the increase of crystal size Fig. 8(a). The degree of order for dolomite crystals of microbial dolomite of the intra-platform mound-shoal environment is greater than 0.7 (0.7–0.98), also considerably higher than that of dolomite crystals related to low-temperature microbial dolomitization (0.4–0.5), which also implies the influences of burial dolomitization and hydrothermal dolomitization in the later stage. To sum up, for the microbial dolomite reservoir of the intraplatform mound-shoal environment, the multi-stage diagenetic evolution pattern Fig. 9 is summarized as below: the microbial carbonate buildup in uplift parts of the micro-geomorphology→contemporaneous microbial dolomitization, and early foliaceous dolomite cementation→penecontemporaneous selective dissolution→burial dolomitization→hydrothermal dolomitization, burial-hydrothermal dissolution, and hydrothermal mineral cementation, which produce the euhedral-subhedral granular dolomite with or without residual textures, subhedral-anhedral fine-to medium granular dolomite with no residual texture, and anhedral medium-to coarse granular dolomite. The dolomite crystals formed in multiple stages of dolomitization present themselves in tight mosaic contact to form the rock framework, while cement or hydrothermal minerals, such as quartz, pyrite, and saddle dolomite, are mainly found as pore fillings.

Fine crystalline carbonate sediments containing argillaceous and terrestrial siliceous detritus are mainly deposited in the low-

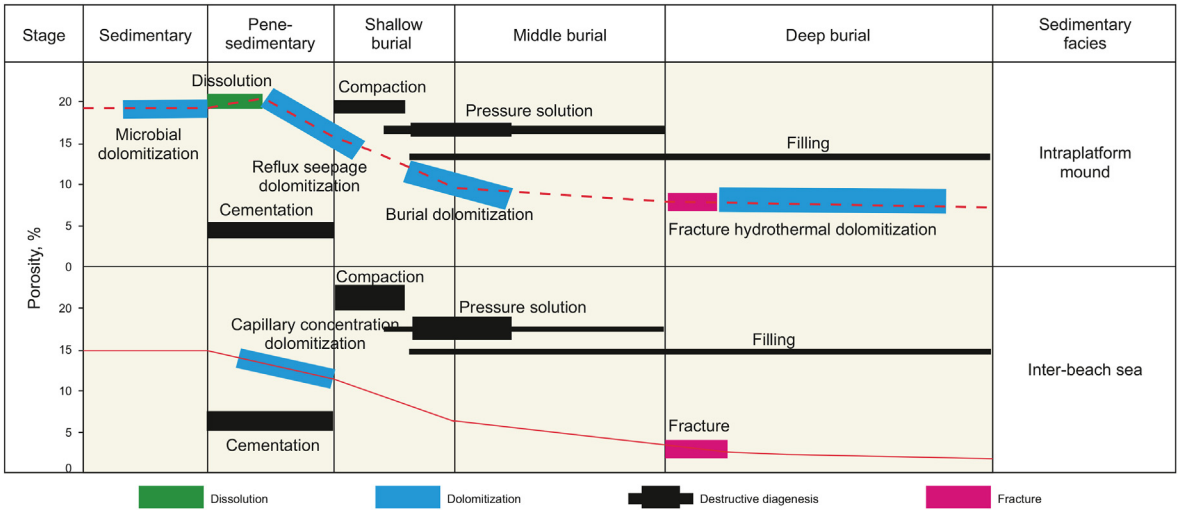

Fig. 9. Relationship between diagenesis and pore evolution of dolomite reservoirs of Z_2dn_4 in Sichuan Basin.

energy still water environment of the inter-beach sea. When the sea level drops, evaporated dolomite is formed in the arid climate. Thus, it is often associated with gypsum nodules or precipitation of cement. Such evaporated dolomite derived from diagenetic replacement as a result of the increase of Mg^{2+} concentration due to the deposition of gypsum, which is also named seepage reflux dolomitization during (pene-)contemporaneous stage (Adams and Rhodes, 1961; Zhao et al., 2018). The gypsum nodules and corresponding moldic pores are only found in a few samples and no regional gypsum-bearing dolomite or gypsum rock is observed, which indicates that seepage reflux dolomitization is limited. The relatively large seawater depth leads to the reduced frequency and probability of sediments exposed to the surface, and thus it is unlikely to have intensive contemporaneous or penecontemporaneous dissolution. Therefore, for low-energy fine crystalline carbonate sediments, they have not suffered from the modification of the near-surface diagenetic environment, and instead, directly enter the shallow burial diagenesis. Because of the weak early dolomitization, the rock framework is still unconsolidated with low stiffness, which cannot effectively resist the mechanical compaction during the burial process. The mechanical compaction greatly reduces the porosity, and the stylolite, reflecting intensive compaction, is also relatively well developed (Fig. 8(d)). Due to the superposition of burial dolomitization, the crystal nucleus does not have enough pore space to grow in the process of replacement and recrystallization, and finally forms anhedral fine crystalline dolomite containing mostly primary inter-crystalline pores. The dolomite crystals are found with a tight mosaic granular texture, and the overall rock is also highly densified. The densification of rock in the diagenesis process also blocked the flow of hydrothermal fluids, and thus suppressed the activity of hydrothermal dolomitization—either of the related dissolution and precipitation processes barely occur. The stable isotope of carbon and oxygen are characterized by the low positive value of δC^{13} and high negative value of δO^{18} Fig. 8(a), attributed to burial dolomitization (Zhao et al., 2018). The diagenetic evolution pattern of the dolomite in the inter-beach sea environment Fig. 9 is concluded as: fine crystalline carbonate deposition containing argillaceous and siliceous materials→weak seepage reflux dolomitization→intensive mechanical compaction and densification→burial dolomitization, resulting in the pore-dominated anhedral fine crystalline dolomite, and also crack-pore dolomite with the superimposed presence of later structural cracks. Due to the absence of eogenetic dolomitization, terrestrial particles, such as clay and quartz, do not only fill the primary pores but also tend to distribute among carbonate particles to form a stable structure, and subsequently take the role as the rock framework together with dolomite crystals via later dolomitization. If the argillaceous or quartz content is high during deposition, interbedding of clay, quartz, and dolomite is anticipated, and the influence of clay and quartz on the elastic properties of rock framework are expected to be more profound Fig. 2(h).

The dolomite in the calcareous dolomite mainly develops along the stylolite, which implies the genetic relationship between them. Moreover, the euhedral crystal morphology also reflects the low-temperature genesis of dolomite. Pressure solution leads to the formation of stylolite, and meanwhile, it can stimulate the release of Mg^{2+} in limestone, which increases the concentration of Mg^{2+} in seawater and promotes the growth of dolomite crystals along the stylolite. Because Mg^{2+} released by pressure solution is not enough to enable complete dolomitization of limestone, which cause the dolomite content variation in the calcareous dolomite. In the meantime, owing to the differentiated dolomitization, dolomitization is not exclusive to the position near the stylolite and some dolomite crystals may be distributed in the limestone matrix.

5.2. Crystal contact boundary and its influence on rock physical properties

After the multi-stage dolomitization diagenetic process, the dolomite crystals of the Z_2dn_4 dolomite generally shows the crystalline texture characteristic. The elastic wave propagates across the whole rock medium through dolomite crystals and their contact boundaries. As the “weak planes” of mechanical properties, the seismic response of the crystal boundary is stronger than that of rigid dolomite crystals, which leads to the decisive effect of the mechanical properties of the crystal boundary on the macroscopic elastic properties of the rock medium. According to the sedimentary and diagenesis processes of rock samples and the rock microtexture characteristics, four types of crystal contact are identified Fig. 10: ① “welding” contact among dolomite crystals, mainly developing in tight anhedral dolomite and subhedral-anhedral dolomite with dissolution pore-vugs, and associated with the boundary mechanical properties nearly equal to those of dolomite crystals; ② clay serving as the dolomite crystal boundary (clay-type crystal boundary), developing in tight anhedral argillaceous dolomite and associated with the mechanical properties affected by the

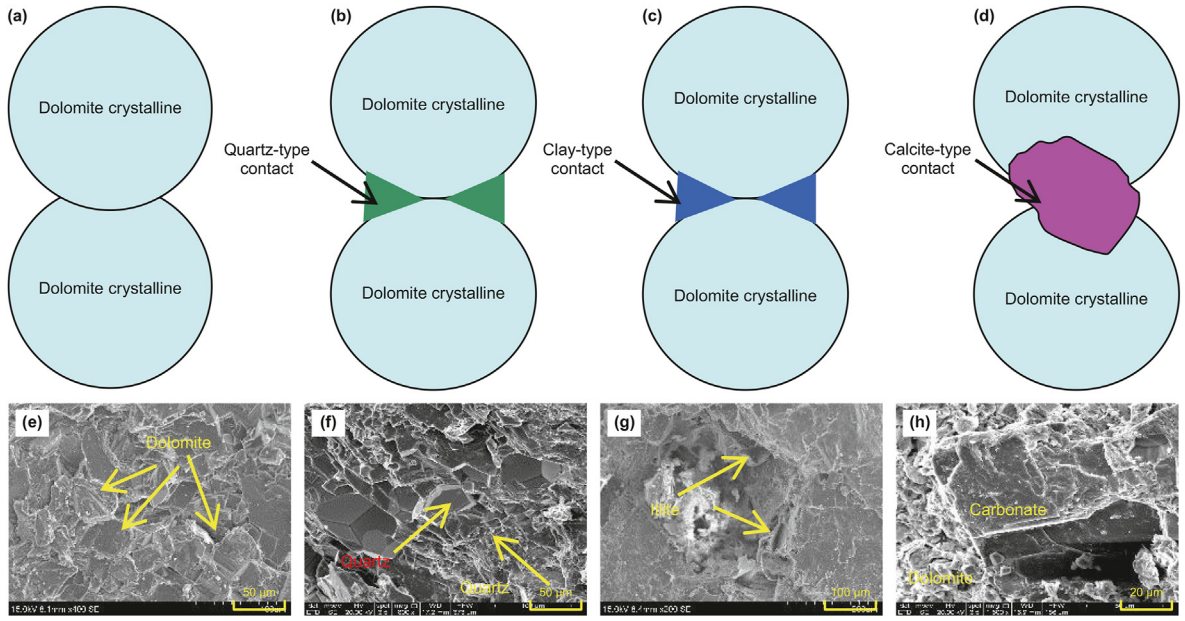

Fig. 10. Conceptual model of crystal contact boundary and SEM images of dolomite grains of the Z_2dn_4: **(a)** "welding" contact of dolomite particles; **(b)** quartz-type crystal boundary; **(c)** clay-type crystal boundary; **(d)** calcite-type crystal boundary; **(e)** dolomite crystals are in "welding" contact; **(f)** quartz-cemented dolomite crystals; **(g)** illite grains at dolomite crystal boundary; **(h)** carbonate crystals in dolomite.

elastic properties of clay particles (clay and dolomite particles jointly serve as the load-bearing framework); ③ quartz cementation serving as the dolomite crystal boundary (interbedding of dolomite and quartz), occurring in the tight anhedral siliceous dolomite and associated with the boundary mechanical properties affected by the elastic properties of quartz particles (quartz and dolomite particles together constitute the load-bearing framework); ④ carbonate grains as the dolomite crystal boundary (calcite-type crystal boundary), present in tight calcareous dolomite and associated with the boundary mechanical properties affected by the elastic properties of carbonate particles (carbonate and dolomite particles both serve as the load-bearing framework). A variety of contact types can be developed in the same sample. For example, the tight argillaceous dolomite may have two boundary types, the clay type crystal boundary and the "welding" contact crystal boundary.

The mechanical properties of crystal boundaries of the samples control the variation of the V_p/V_s ratio (in other words, the Poisson's ratio and V_p–V_s relationship) with the P-wave velocity. With the change of the predominance of crystal boundaries from the siliceous (quartz) cementation contact → "welding" dolomite crystal contact to finally clay- and calcite-crystal boundaries, the V_p/V_s ratio of the dry samples presents an overall gradual increasing tendency Fig. 7(b), which actually reflects the V_p/V_s ratio of crystal boundary minerals, among them quartz grain showing the minimum V_p/V_s ratio and clay, carbonate grain showing the maximum ratio V_p/V_s ratio. Clearly, the acoustic velocity is affected by mineral composition. The increasing content of quartz, calcite, and clay in the sample all leads to considerable declines of the P- and S-wave velocities Fig. 8. The main reason behind this phenomenon is still that with the increasing quartz, clay, and calcite, the content of the crystal boundaries with weaker elastic properties in the rock crystal framework gradually increases. The modulus of the sample is affected by the crystal boundary. The modulus of the welded contact boundary is close to the modulus of the dolomite crystal. The bulk modulus of the quartz-type crystal boundary, clay-type crystal boundary and calcite-type crystal boundary is affected by quartz, clay and calcite. The modulus moves closer to quartz (bulk modulus: 37 GPa, shear modulus: 44 GPa), clay (bulk modulus: 25 GPa, shear modulus: 9 GPa) and calcite (bulk modulus: 76.8 GPa, shear modulus: 32 GPa), thus affecting the seismic elastic properties of the samples (Mineral modulus value reference Mavko et al., 2023). It is necessary to emphasize that here is a qualitative analysis based on the elastic measurement results and microstructure analysis of the sample, and the SEM image of the sample proves this conclusion. However, the quantitative relationship between bulk modulus (shear modulus) and grain boundary has not been established, which is also the next research direction.

5.3. The links between rock types and rock physical properties

To further discuss the links between diagenesis/rock types and rock physical properties, the correlation between the P- and S-wave velocities of the dolomite samples of the Z_2dn_4 is illustrated in Fig. 11(a). For comparative purposes, the predicted results of the mudrock line model representing the P/S-wave velocity relationship of clastic sandstone (Mavko et al., 2023), and those of the limestone ($V_p = 1.9V_s$) and dolomite ($V_p = 1.82V_s$) models are also plotted (in curves). It can be seen that the measurement points of the dolomite samples, located between the mudrock line and limestone line, present no overall statistical relationship. The correlation between the P- and S-wave velocities of the samples is considerably dependent on the rock composition. We can observe that the samples of the argillaceous dolomite, siliceous dolomite, calcareous dolomite, and the relatively pure crack-dissolution vug and dissolution vug dolomite samples show a linear P- and S-wave velocity correlation, respectively, which reflects the control of the mechanical properties of the boundary of rock particles (crystals). The limestone and dolomite model line represent the P- and S-wave velocity relationships of the calcite and dolomite crystals, respectively, and similarly, the line of the clastic sandstone is the embodiment of that of the quartz framework. The linear P- and S-wave velocity correlations of the argillaceous and calcareous dolomite samples gradually approach the limestone line, with the

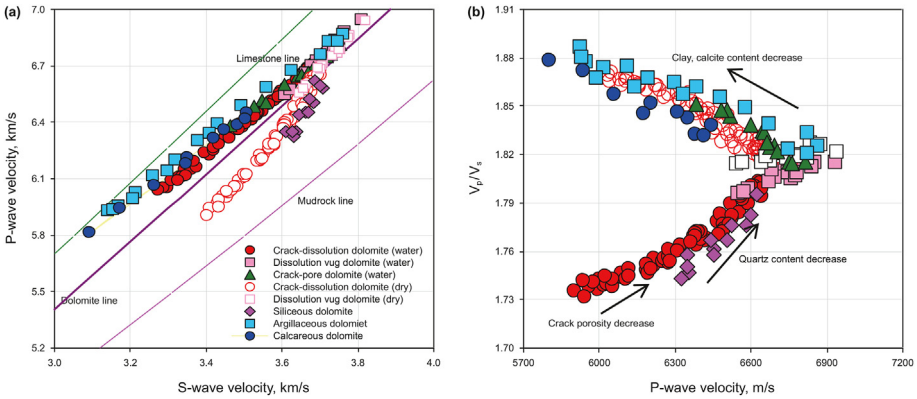

Fig. 11. P-wave velocity versus S-wave velocity **(a)** and P-wave velocity versus V_p/V_s ratio **(b)** of samples in Z_2dn_4.

increasing content of clay and calcite, which implies the gradual increase of the clay and calcite content in samples. However, the siliceous dolomite line gradually approaches the clastic sandstone line, with the growing quartz content. For the crack-dissolution vug and dissolution vug dolomite samples, the corresponding P- and S-wave velocity relationships are close to that of dolomite crystals (dolomite line), which, yet, gradually deviates from the dolomite line with the increasing content of compliant pores such as cracks and pore throats. The stiffness of soft pores like cracks greatly increases after water saturation, which, combined with the squirt flow-related velocity dispersion, results in the P-wave velocity growth much more than that of the S-wave velocity. Therefore, with the increasing soft pores in the crack-dissolution vug dolomite samples, the P- and S-wave velocity correlation under the water-saturated condition shifts toward the limestone line. For the dry conditions, the increasing content of soft pores leads to a greater decline of the P-wave velocity, and thus the corresponding P- and S-wave velocity relationship deviates toward the clastic sandstone line. Because the dissolution vugs feature higher intrinsic rigidity, the fluid change has no notable effect on the pore rigidity. Moreover, the variation of the dissolution vug content has the same influences on the P- and S-wave velocities. Consequently, the P- and S-wave velocity relationship of the dissolution vug samples with relatively is still close to the dolomite line, even though the pore-saturated fluid changes or the dissolution pore-vug content varies.

As a result of P- and S-wave velocity correlation under dry and water-saturated condition, the P-wave velocity declines gradually with the increasing content of quartz, clay, and calcite, and furthermore, the velocity ratio (V_p/V_s) in the siliceous dolomite samples gradually climbs up, with the growing P-wave velocity. However, the argillaceous and calcareous dolomite samples present the opposite variation tendencies, which lead to a counterclockwise-90°-rotated V-shaped overall correlation between the P-wave velocity and the velocity ratio Fig. 11(b). Due to the difference of the effects of cracks on P- and S-wave velocities for dry and water-saturated samples, the P-wave velocity and the velocity ratio of dry samples decreases gradually with the increasing cracks, while the P-wave velocity of water-saturated samples declines gradually with the increasing cracks, yet accompanied by the growing velocity ratio. In particular, the P-wave velocity and velocity ratio of dry samples with high content of cracks are even lower than those of siliceous dolomite. The mechanical properties of soft pore throats are similar to those of cracks, and the influences of their content changes on the P-wave velocity and velocity ratio are the same as those of cracks. The relatively rigid dissolution vugs are found with no notable change of pore rigidity, caused by pore fluid changes. Therefore, the dissolution vug and pore-dominated samples (with lower overall porosity) present only minor differences in the acoustic velocity between dry and water-saturated conditions, and the relationship between the P-wave velocity and velocity ratio is also observed with no considerable change.

5.4. The implications for deep burial carbonate reservoir prediction

Deep-ultra-deep carbonate rock is one of the important oil and gas exploration objects at present and in the future, and experienced the strong influence of multi-cycle tectonic evolution. It has the characteristics of old age, deep burial, strong diagenesis and strong reservoir heterogeneity (obvious changes in rock characteristics in vertical and horizontal directions). Through the systematic rock physics experiment of dolomite in the Z_2dn4 under the geological framework, we determined the difference of reservoir petrological characteristics caused by multi-stage diagenesis, discussed the influence and control of geological factors on the rock physical characteristics of shale samples. On this basis, the evolutionary relationship among geological process, reservoir rock structure evolution and seismic elastic response mode was established, which gave more accurate geological indication significance to seismic rock physics characteristics, expanded the connotation of seismic rock physics research, and improved the accuracy of seismic and logging evaluation. As a reference example, this experimental research model also helps to solve the problem that it is difficult to accurately identify the multi-stage superposition of deep fluids in the oil and gas exploration of other similar deep-ultra-deep carbonate rocks.

6. Conclusions

The diagenesis of the dolomite in the Z_2dn_4 reservoir is mainly controlled by the depositional environment. The microbial dolomite of the high-energy mound-shoal environment is subjected to the contemporaneous microbial dolomitization, seepage reflux dolomitization, (pene-)contemporaneous selective dissolution, burial dolomitization, and hydrothermal dolomitization, successively. The resultant crystalline dolomite of multi-stage dolomitization is found mainly of compact “welding” contact dolomite crystal boundaries. The pores are mainly derived from the inheritance of the primary pores and (pene-)contemporaneous dissolution. With the good coordination of pore throats and crack that improve connection with dissolved pore-vugs, the pore throat and cracks both serve as the fluid flow channels.

The siliceous, argillaceous, and calcareous dolomite of the inter-beach sea environment primarily undergo the weak seepage reflux dolomitization, intensive mechanical compaction-induced

densification, and burial dolomitization, which form the tight anhedral silty-to fine crystalline dolomite. Such crystalline dolomite formed by multi-stage dolomitization is found with four types of crystal contact boundaries, namely the compact "welding" contact, clay-type, quartz cementation-type, and calcite-type. The porosity is mainly attributed to residual primary inter-granular or crystalline pores, and crack take the role as the main fluid flow channel. The porosity-permeability relationship represents the crack-dependent linear seepage.

The mechanical properties of the crystal boundary and pore structure characteristics jointly control the variation of the seismic elastic properties such as the relationship between the P-wave velocity and the V_p/V_s ratio, and porosity-velocity correlation. With the increase of the siliceous cementation crystal boundaries, the linear P- and S-wave velocity relationship deviates from the dolomite model line to the clastic sandstone model line, associated with declines of both the P-wave velocity and V_p/V_s ratio. Moreover, with the growing content of clay- and calcite-type crystal boundaries, the linear P- and S-wave velocity relationship deviates from the dolomite model line to the limestone model line, accompanied by the decline of the P-wave velocity and yet the growth of the V_p/V_s ratio. For dry samples, the acoustic velocity and velocity ratio decrease with the growing content of soft pores like cracks. However, in the case of water-saturated samples, the acoustic velocity declines, and the V_p/V_s ratio grows, with more soft pores. Without considering the mechanical properties of crystal contact boundaries, the porosity-velocity relationship of the dolomite samples is primarily controlled by the pore structure, followed by porosity as the secondary factor.

Conflict of interest

The authors declare that they have no known competing financial interests or personal relationships that could have appeared to influence the work reported in this paper.

CRediT authorship contribution statement

Chuang Li: Writing – original draft. **Shu-Xin Pan:** Methodology. **Hong-Bin Wang:** Software. **Ji-Xin Deng:** Data curation. **Jian-Guo Zhao:** Writing – review & editing. **Zhi Li:** Formal analysis. **Yu Zhang:** Methodology.

Acknowledgments

This study is funded by the CNPC (China National Petroleum Corporation) Scientific Research and Technology Development Project (Grant No. 2023ZZ0205, 2021DJ0506). This work is sponsored by the National Natural Science Foundation of China (41774136, 41374135). We thank Zhong-Hua Xu for providing the technical support on SEM and thin sections. The data used for building figures and relevant imaging may be obtained by contacting the co-author (dengjixin@cdut.cn).

References

Adams, J.E., Rhodes, M.L., 1961. Dolomitization by seepage refluxion. AAPG (Am. Assoc. Pet. Geol.) Bull. 44 (12). https://doi.org/10.1306/0BDA6263-16BD-11D7-8645000102C1865D, 1921–1920.

Anselmetti, F.S., Eberli, G.P., 1999. The velocity-deviation log: a tool to predict pore type and permeability trends in carbonate drill holes fromsonic and porosity or density logs. AAPG (Am. Assoc. Pet. Geol.) Bull. 83, 450–466. https://doi.org/10.1306/00AA9BCE-1730-11D7-8645000102C1865D.

Ba, J., Carcione, J.M., Nie, J.X., 2011. Biot-Rayleigh theory of wave propagation in double-Porosity media. J. Geophys. Res. Solid Earth 116, B06202. https://doi.org/10.1029/2010JB008185.

Chen, Y.N., Shen, A.J., Pan, L.Y., et al., 2017. Features, origin and distribution of microbial dolomite reservoirs: a case study of 4th Member of Sinian Dengying Formation in Sichuan Basin, SW China. Petrol. Explor. Dev. 44 (5), 704–715. https://doi.org/10.1016/S1876-3804(17)30085-X.

Choquette, P.W., Pray, L.C., 1970. Geologic nomenclature and classification of porosity in sedimentary carbonates. AAPG (Am. Assoc. Pet. Geol.) Bull. 54, 207–250. https://doi.org/10.1306/5D25C98B-16C1-11D7-8645000102C1865D.

Deng, J.X., Wang, H., Zhou, H., et al., 2015a. Microtextural, seismic rock physical properties and modeling of Longmaxi Formation shale. Chin. J. Geophys. 58 (6), 2123–2136. https://doi.org/10.6038/cjg20150626 (in Chinese).

Deng, J.X., Zhou, H., Wang, H., Zhao, J.G., Wang, S.X., 2015b. The influence of pore structure in reservoir sandstone on dispersion properties of elastic waves. Chin. J. Geophys. 58 (9), 3389–3400. https://doi.org/10.6038/cjg20150931 (in Chinese).

Du, J.H., Wang, Z.C., Zou, C.N., et al., 2015. Geologic Theory and Exploration Practice of Ancient Large Carbonates Gas Field. Petroleum Industry Press, Beijing.

Guo, J.X., Gurevich, B., Chen, X.F., 2022. Dynamic SV-wave signatures of fluid-saturated porous rocks containing intersecting fractures. J. Geophys. Res. Solid Earth 127 (8), e2022JB024745. https://doi.org/10.1029/2022JB024745.

He, Z.L., Ma, Y.S., Zhu, D.Y., et al., 2021. Theoretical and technological progress and research direction of deep and ultra-deep carbonate reservoirs. Oil Gas Geol. 42 (3), 533–546. https://doi.org/10.11743/ogg20210301.

Hu, Z.D., He, Z.H., Liu, W., et al., 2016. Scalar wave equation modeling using the mixed-grid finite-difference method in the time-space domain. Chin. J. Geophys. 59 (10), 3829–3846. https://doi.org/10.6038/cjg20161027.

Jiang, L., Hu, A.P., Ou, Y.L., et al., 2023. Diagenetic evolution and effects on reservoir development of the Dengying and Longwangmiao formations, central Sichuan Basin, Southwestern China. Petrol. Sci.

Jin, Z.J., Cai, L.G., 2006. Exploration propects, problems and strategies of marine oil and gas in China. Oil Gas Geol. 27 (6), 722–727. https://doi.org/10.11743/ogg20060602 (in Chinese).

Kong, L.Y., Wang, Y.B., Yang, H.Z., 2013. Wavefield propagation characteristics in fracture-induced TTI double-porosity medium. Acta Phys. Sin. 62 (13), 555–564. https://doi.org/10.7498/aps.62.139101.

Li, J., She, Y.Q., Gao, Y., Yang, G.R., Li, M.P., Yang, S., 2019. Onshore deep and ultra-deep natural gas exploration fields and potentials in China. China Petrol. Explor. 24 (4), 403–417. https://doi.org/10.3969/j.issn.1672-7703.2019.04.001.

Li, S.Q., Wang, W.H., Su, Y.D., et al., 2023. Effective elastic properties and shear-wave anisotropy for rocks containing any oriented penny-shaped cracks in transversely isotropic background. Geophysics 88 (3), MR65–MR81. https://doi.org/10.1190/geo2022-0388.1.

Liao, J.P., Wen, P., Guo, J.X., et al., 2023. Seismic dispersion, attenuation, and frequency-dependent anisotropy in a fluid-saturated porous periodically layered medium. Geophys. J. Int. 234 (1), 331–345. https://doi.org/10.1093/gji/ggad080.

Ma, X.H., Yang, Y., Wen, L., et al., 2019a. Distribution and exploration direction of medium- and large-sized marine carbonate gas fields in Sichuan Basin, SW China. Petrol. Explor. Dev. 46 (1), 1–13. https://doi.org/10.1016/S1876-3804(19)30001-1.

Ma, Y.S., He, Z.L., Zhao, P.R., et al., 2019b. A new progress in formation mechanism of deep and ultra-deep carbonate reservoir. Acta Pet. Sin. 40 (12), 1415–1425 doi: CNKI:SUN:KTSY.0.2020-03-014.

Ma, Y.S., Li, M.W., Cai, X.Y., et al., 2020. Mechanisms and exploitation of deep marine petroleum accumulations in China: advances, technological bottlenecks and basic scientific problems. Oil Gas Geol. 41 (4), 655–683. https://doi.org/10.11743/ogg20200401.

Mavko, G., Mukerji, J., Dvorkin, J., 2023. The Rock Physics Handbook: Tools for Seismic Analysis in Porous Media. Cambridge University Press, New York, pp. 1–329.

Wang, Z.Z., Schmitt, D.R., Wang, R.H., 2015a. Does wettability influence seismic wave propagation in liquid-saturated porous rocks? Geophys. J. Int. 203, 2182–2188. https://doi.org/10.1093/gji/ggv434.

Wang, Z.Z., Wang, R.H., Wang, F.F., et al., 2015b. Experiment study of pore structure effects on velocities in synthetic carbonate rocks. Geophysics 80 (3), D207–D219. https://doi.org/10.1190/geo2014-0366.1.

Wang, W.Z., Yang, Y.M., Wen, L., et al., 2016. A study of sedimentary characteristics of microbial carbonate: a case study of the Sinian Dengying Formation in Gaomo area, Sichuan basin. Chin. Geol. 43 (1), 306–318 (in Chinese with English abstract). doi: CNKI:SUN:DIZI.0.2016-01-023.

Wang, Z.Z., Njiekak, G., Schmitt, D.R., et al., 2021. Empirical rock physics relationships on carbonate dry-frame elastic properties. Petrol. Sci. 18 (3), 24. https://doi.org/10.1007/s12182-021-00565-y.

Warthmann, R., Vasconcelos, C., Sass, H., et al., 2005. Desulfovibrio brasiliensis sp. nov., a moderate halophilic sulfate-reducing bacterium from Lagoa Vermelha (Brazil) mediating dolomite formation. Extremophiles 9 (3), 255–261. https://doi.org/10.1007/s00792-005-0441-8.

Weger, R.J., Eberli, G.P., Baechle, G.T., et al., 2009. Quantification of pore structure and its effect on sonic velocity and permeability in carbonates. AAPG (Am. Assoc. Pet. Geol.) Bull. 93, 1297–1317. https://doi.org/10.1306/05270909001.

Xie, J.Y., Zhang, J.J., Xiang, W., et al., 2022. Effect of microscopic pore structures on ultrasonic velocity in tight sandstone with different fluid saturation. Petrol. Sci. 19 (6), 2683–2694. https://doi.org/10.1016/j.petsci.2022.06.009.

Yang, H.J., Chen, Y.Q., Tian, J., et al., 2020. Great discovery and its significance of ultra-deep oil and gas exploration in well Luntan-1 of the Tarim Basin. China Petrol. Explor. 25 (2), 62–72. https://doi.org/10.3969/j.issn.1672-7703.2020.02.007.

Yin, X.Y., Zong, Z.Y., Wu, G.C., 2015. Research on seismic fluid identification driven by rock physics. Sci. China Earth Sci. 58, 159–171. https://doi.org/10.1007/s11430-014-4992-3.

Zhang, S.C., Zhu, G.Y., He, K., 2011. The effects of thermochemical sulfate reduction on occurrence of oil-cracking gas and reformation of deep carbonate reservoir and the interaction mechanisms. Acta Petrol. Sin. 27 (3), 809–826. https://doi.org/10.7623/syxb201304012.

Zhao, W.Z., Wang, Z.C., Hu, S.Y., et al., 2012. Large-scale hydrocarbon accumulation factors and characteristics of marine carbonate reservoirs in three large onshore cratonic basins in China. Acta Pet. Sin. 33 (S2), 1–9. https://doi.org/10.1016/j.matlet.2012.03.097.

Zhao, L., Nasser, M., Han, D., 2013. Quantitative geophysical pore-type characterization and its geological implication in carbonate reservoirs. Geophys. Prospect. 61, 827–841. https://doi.org/10.1111/1365-2478.12043.

Zhao, W.Z., Shen, A.J., Qiao, Z.F., et al., 2018. Genetic types and distinguished characteristics of dolomite and the origin of dolomite reservoirs. Petrol. Explor. Dev. 45 (6), 923–935 doi: CNKI:SUN:PEAD.0.2018-06-002.